WIND TUNNEL MEASUREMENTS OF AERODYNAMIC INTERACTIONS BETWEEN HELICOPTERS

P J Skinner and J C F Martins
Defence Aeronautics Programme, Defencetek, CSIR
pskinner@csir.co.za, jmartins@csir.co.za

Abstract

Wind tunnel measurements of the aerodynamic interactions between two helicopters are presented. The measured results include the force and moment changes on the downwind helicopter as a function of its position relative to the upwind helicopter (longitudinal, lateral, and vertical). The magnitudes and locations of the interactions are clearly visible. Favourable interaction regions are explored with controlled tethered flight to confirm the power reduction potential.

Nomenclature

A = rotor disc area, m^2

c = Chord, m

cg = centre of gravity

C_D, cd = drag coefficient, $\frac{fd_w}{\rho A(\omega R)^2}$

C_Y, cy = cross wind coefficient, $\frac{fcw_w}{\rho A(\omega R)^2}$

C_T, ct = thrust coefficient $\approx \frac{fl_w}{\rho A(\omega R)^2}$

C_l, cll = roll moment coefficient, $\frac{mll_w}{\rho A(\omega R)^2 R}$

C_m, clm = pitch moment coefficient, $\frac{mlm_w}{\rho A(\omega R)^2 R}$

C_n, cln = yaw moment coefficient, $\frac{mln_w}{\rho A(\omega R)^2 R}$

C_P = power coefficient, $\frac{Power}{\rho A(\omega R)^3}$

D = rotor diameter, m

fl_w = wind axis lift force, N

fcw_w = wind axis cross wind force, N

fd_w = wind axis drag force, N

mll_w = wind axis roll moment, Nm

mlm_w = wind axis pitch moment, Nm

mln_w = wind axis yaw moment, Nm

mrc = moment reference centre

R = rotor radius, m

RC = Radio Controlled

V_∞ = Wind Tunnel Free Stream Velocity, m/s

VFR = Visual Flight Rules

X = longitudinal axis, positive upwind

Y = lateral axis, positive to starboard

Z = vertical axis, positive upwards

α = Angle of Attack, °

Δ (…) = change in (…)

μ = advance ratio, $\frac{V_\infty}{\omega R}$

ψ = azimuth clockwise, deg (0° forward)

ρ = air density (kg/m^3)

σ = Rotor solidity, $\frac{N c}{\pi R}$ (sigma)

ω = rotational speed (rad/s)

Introduction

This effort was co-funded by the AMRDEC group of the US Army through the European Research Office of the US Army. The work was carried out under the leadership of Dr C Tung of AMRDEC.

In contrast to aircraft, relatively little is known concerning the intermediate and far field wake of rotorcraft and the interference effects of these wake structures. Much effort has been spent on characterising the near field wakes from the main rotor to better understand effects that influence rotor performance so that improvements in rotor design may be made. An example of this is the work described by Ghee et al (Ref 1). The CSIR is conducting a series of wind tunnel tests to characterise the intermediate rotorcraft wake as described by Denton et al (Ref 2) and interference effects between rotorcraft as described below.

A significant amount of work has been carried out to study the hazardous effects of wake interactions between fixed wing aircraft and example of which is

described by Vicroy et al (Ref 3). The effects of fixed wing aircraft flying in close proximity to each other have also been described by Hansen and Cobleigh (Ref 4).
Not many studies, however, appear to have been carried out experimentally on the effects of wake interference between rotorcraft. Interference effects between models of two tilt-rotor aircraft have however been carried out by Johnson et al (Ref 5). The work described herein will be of a similar nature to that described by Johnson but using models of helicopters rather than tilt-rotors.

The testing that has been performed to date is for two helicopters operating at similar thrust coefficients at low advance ratios. The static aerodynamic interference has been quantified as well as first order operational implications of the interference through controlled trimmed tethered flight in the interference flow-field.

The objective is to achieve increased understanding of aerodynamic rotorcraft interference effects as it applies to rotorcraft formation flight and wake encounters.

Test Apparatus

Two radio controlled (RC) helicopter models were installed in the Seven Metre Wind-tunnel (7.5mx6.5m) at CSIR, South Africa (Figure 1). The helicopter models used were fully articulated 46-size RC models of the Agusta A109 helicopter.

The four bladed main rotors rotated in the clockwise sense when viewed from above. The blades were made from glass fibre and had a 21% cut-out and up to 94% radius had constant chord (48mm); constant thickness (~16%) and zero twist. The blade tips comprised 2-stage compound linear taper providing a rotor diameter of 1318mm.

The fully articulated main rotors had collective and cyclic control. Spherical bearings at the cuff allowed for limited flapping and the attachment hinges allowed for lead/lag motion. The 2-bladed tail rotors had collective control and lead/lag hinges. Each helicopter was attached to a 6-component balance for the measurement of the forces and moments. Space constraints dictated that the balance assemblies were located below the fuselage. Initial concerns that the roll moment range of the small balances may have been exceeded were addressed by allowing the models to rotate on bearings about the balance longitudinal axes. Appropriate hard stops were included to limit the allowable roll angle ranges. The roll degree of freedom of the downwind helicopter could be removed by a clamping device. A pitch axis was included below each balance assembly which was driven by an electric motor through a worm drive. Similarly a yaw axis was included for the downwind helicopter to cater for yawed flight in subsequent testing (not done in these tests). (Figure 2)

Brushless DC electric motors were used to drive the helicopter rotors through the standard clutch assemblies. Power was supplied from an external DC power supply which required significant capacitor treatment to smooth out ripple on the line. The main rotor test speed was approximately 1200 RPM yielding tip speeds of about 83 m/s and tip Reynolds numbers of about 220 000.

The helicopter models were mounted to the balance assemblies using rubber dampers which proved essential to eliminate ground resonance effects.

The helicopter aerodynamic interaction investigation was performed with two helicopter models by operating the downwind helicopter in the wake of the upwind helicopter. The upwind helicopter was mounted on a fixed strut at zero angle of yaw. The wind tunnel's integral overhead XYZ traverse system (Figure 1) was used to support and position the downwind helicopter at the required longitudinal, lateral, and vertical locations relative to the fixed upwind helicopter for the tests.

A computer was used to control the RC helicopters by supplying analogue control signals to control channels on the radios which were transmitted to the helicopters. The standard RC receivers were used with external power supplies. The models were free to roll and were trimmed to specified roll angles, using lateral cyclic. The 6-component strain gauge balances measured the aerodynamic forces on the model and the fuselage pitch and roll angles were measured by potentiometers.

Software control loops used feedback from the balances and attitude potentiometers to drive the control hardware to achieve trimmed flight for each case according to the arrangement in Table 1. A relatively high control loop frequency was required for the lateral cyclic due to the models being free to roll. These two channels were operated off a separate hardware system with an update frequency of about 35 Hz which proved adequate. The remaining control loops were less critical and operated at 10 to 15 Hz. The tethered nature of the support system meant that the response was entirely unrealistic. The pitch motion had to be supplied by a motor and there was no yaw motion allowed.

The initial focus of these tests was on changes from trim due to the aerodynamic interaction and less on the absolute value of the trim attitude. Subsequent testing was performed where the downwind helicopter was trimmed while it was traversed through the wake from the upwind helicopter with the objective of measuring the helicopter power. For these tests an ammeter was used to record the current drawn by the downwind helicopter to determine the power helicopter power. The supply voltage to the electric motors was constant.

The origin of the coordinate system was the centre of upwind helicopter rotor disc. The downwind

helicopter position (x,y,z) was expressed relative to this origin. All positions are expressed in terms of the rotor diameter, D. A negative x position refers to downwind distance. The lateral position (y) is positive with the downwind helicopter to starboard of the upwind helicopter. The vertical position (z) is positive with the downwind helicopter above the upwind helicopter.

The three force and three moment coefficients available from the 6-component strain gauge balance were recorded in these tests (convention when looking upwind from behind the helicopter):

$$C_D = \frac{fd_w}{\rho A(\omega R)^2}\text{ ; + downwind}$$

$$C_Y = \frac{fcw_w}{\rho A(\omega R)^2}\text{ ; + to starboard}$$

$$C_T' = \frac{fl_w}{\rho A(\omega R)^2} \approx C_T\text{ ; + up}$$

$$C_l = \frac{mll_w}{\rho A(\omega R)^2 R}\text{ ; + starboard side down}$$

$$C_m = \frac{mlm_w}{\rho A(\omega R)^2 R}\text{ ; + nose up}$$

$$C_n = \frac{mln_w}{\rho A(\omega R)^2 R}\text{ ; + nose to starboard}$$

The forces and moments refer to net loads, i.e. the effects of model mass have been removed and the moments have been transferred to the required mrc for the helicopters.

The Seven Metre Wind-tunnel facility is an open return type with a small contraction and is therefore sensitive to changes in ambient conditions. Speed control is by selection of various constant speed fan patterns (Figure 1) and the speed cannot be altered to compensate for ambient wind changes. Therefore a degree of variability in the test data is to be expected particularly at the low advance ratios and thrust coefficients used for testing.

Table 1: Helicopter control architecture

Helicopter channel	**Feedback signal**
Main rotor collective	Net lift force
Tail rotor collective	Net yaw moment about mrc
Longitudinal cyclic	Net drag force
Roll angle	Net side force
Lateral cyclic	Roll angle / (Side force when roll angle is fixed)
Pitch angle	Net pitch moment about mrc
Throttle	Main rotor RPM

Test Procedure

The models had to be operated in a similar sequence to free flying helicopters to avoid rotor instability i.e. the rotors first had to be brought up to speed; then collective was applied and a controlled hover state was achieved; then the wind tunnel speed was set while the helicopters transitioned into forward flight at which stage testing could commence.

With the upwind helicopter non operational, an approximate trim condition was established for the downwind helicopter at the required thrust setting using the control loops. The roll angle required for this condition was recorded and the helicopter and wind tunnel was shut down. The roll angle of the downwind helicopter was then clamped at the above trim setting angle. Both helicopters were then started and the normal start-up sequence described above was followed. Note that in this case, the downwind helicopter was not in proper trim until the appropriate wind tunnel speed was reached due to the fixed roll angle. This process was required because the rig was not equipped with an automatic locking mechanism for the roll angle.

For the tests, the upwind helicopter was continuously trimmed to a specified thrust and zero moments about the mrc. The downwind helicopter controls and attitude were kept constant at the approximate trim condition determined above. The aerodynamic interaction was manifest on the downwind helicopter by changes in the force and moment coefficients from the initial trim conditions determined above, while the helicopter was traversed in vertical planes through the wake from the upwind helicopter. The pattern of the traverse in the vertical plane is shown in Figure 3 and the definition of the coordinate system is described in Figure 4.

The test conditions relevant here are listed in Table 2.

Table 2 Test conditions

σ	0.093
C_T'/σ	0.035
μ	0.05, 0.10
RPM	1200
x/D	-1.5, -2, -3, -4
y/D	±(0.38 to 1.3)
	-1.3 to 1.3
dy/dt, mm/s	16 , 24
z/D	-1 to 0.15

Further tests were also carried out to quantify any beneficial effects on power from flying a helicopter in the wake region of another helicopter. These tests required a different test philosophy. Power would be determined by measuring motor current and rotational speed. The current was directly proportional to torque and could thus be calibrated. The helicopter control settings were also different. For the power to be representative, the downwind helicopter needed to maintain trimmed flight at the required test conditions such so that the power measured in this condition would be representative of the interference effects on power.

Therefore, for these tests the downwind helicopter was positioned as far to the side as possible from the upwind helicopter. Both helicopter models were then started up as described above. Once the helicopters were trimmed at the desired thrust value, the wind tunnel was started and the helicopter controls were adjusted accordingly to achieve trimmed flight at the desired tunnel speed and thrust.

Once trimmed flight had been achieved on each helicopter then the downwind helicopter was traversed through the wake of the upwind helicopter in the desired pattern. During this process, the control loops continuously maintained trimmed flight. The forces and moments recorded should then remain nominally constant but the measured power required to maintain trimmed flight would then quantify the influence of wake interference on power.

The primary traversing axis for the plane scans was the y-axis. This was traversed at ~24 mm/s which was adequate for measuring the wake interference loads when the controls and attitudes were fixed. This traverse rate was too great, however, for the control loops to maintain trim during the power reduction measurements, resulting in a significant lag in the helicopter response, and the rate was reduced to ~16 mm/s.

The logged data was suitably filtered and data at regular discreet intervals was extracted to produce contour plots of the aerodynamic interaction. The resultant resolution of the sampled regions was 100x100mm (~0.075D).

Results

Interference between two rotor systems was measured with the downwind helicopter in the region of 1.5 to 4 diameters downwind of the upwind helicopter and for lateral separations of 1.3 diameters either side of the upwind helicopter. The vertical measurements varied from 0.15 diameters above to 1 diameter below the upwind helicopter. The tests reported on here are for C_T'/σ = 0.035 and μ = 0.05, 0.10.

The fundamental features of the wake interaction are illustrated in the schematic of Figure 5. Trailing from either side of the upwind helicopter rotor disc are two counter-rotating vortices with the sense indicated. Between these vortices lies the general downwash that is induced through the rotor disc. These flow features are convected downwards with increasing distance downwind by the general downwash action. A helicopter traversing this wake system from port to starboard will initially experience an upwash outboard of the port trailing vortex, followed by a steadily increasing downwash on the opposite side of the vortex which peaks when the two helicopters are longitudinally aligned. Here the downwind helicopter operates in the full downwash from the upwind helicopter. Further motion to starboard will see the downwash reducing and another upwash will be experienced outboard of the starboard trailing vortex. The interaction will be manifest as changes from trim in the downwind helicopter. Primary interactions such as lift changes are expected, but coupled effects due to the rotor blade flapping dynamics should also be present.

It was determined from initial scans that repeatable results were achievable by logging data continuously while the traversing motion was being performed. Figure 6 shows the result of 2 logged lateral passes. The testing was performed by traversing the downwind helicopter laterally from port to starboard and back again at 1.3D downwind and 0.38D below the upwind helicopter.

All of the forces and moments are seen to be affected by the wake from the upwind helicopter. Note that there are small offsets from trim due to test section variability from when the initial trim was performed, errors in the manual fixing of the roll angle, temperature drift effects, etc. The wake interference should be interpreted from the trends in the data.

There are two expected maxima in C_T'/σ at approximately 1D on either side of the upwind helicopter corresponding to the upwash outboard of the trailing vortex pair. The maxima in C_T'/σ at $\pm$1D are accompanied by clear local maxima/minima in several of the other components. C_m/σ experiences a local minimum at y = -1D and a maximum at y = 1D which can be attributed to the blade flapping. At y = -1D the retreating blade is encountering upwash from the trailing vortex. If the maximum upwash, and therefore local blade incidence, occurs at ψ = 90°, the blade will respond by flapping upwards to a maximum at ψ = 180° producing a forward tilt in the rotor disc. This corresponds to a reduced (more negative) C_m/σ which increases the forward thrust component from the rotor and produces the local minimum in C_D/σ (the negative value indicates positive thrust). A similar argument applies to the C_m/σ maximum at

y = 1D except that, due to the advancing blade encountering the upwash, the rotor disc is tilted rearwards, increasing C_m/σ and C_D/σ.

The local maximum and minimum in C_m/σ that occur at ~±0.5D represent a reversal of the response occurring at ±1D. The reason for this may be argued along similar lines except that the upwash has been replaced by the main rotor downwash.

The fluctuations in C_m/σ during the lateral wake encounter have been argued from the perspective of rotor dynamics and should be expected considering the wake interference velocity gradients will be greater laterally across the disc (y-axis) than longitudinally (x-axis). The blade flapping will result in the rotor disc response being greatest along the longitudinal axis and hence the variation in C_m/σ. Similar responses have been predicted using a quasi-static model of helicopter-vortex wake encounters (Ref 6).

The C_l/σ response is significantly less C_m/σ and is less well understood. Using the flapping argument for C_m/σ, the response in C_l/σ indicates greater downwash over the forward section rotor disc which would result in a rotation of the disc towards starboard. Such cases exist when the helicopter lies "further downwind" than the downwash, i.e. the downwash leads the helicopter. The reverse would be expected to apply when the downwind helicopter leads the downwash. Additional transients would also be expected for when the downwind helicopter lies outside the downwash on the port and starboard sides of the wake vortex pair. Figure 6 only shows a transient at y = 1D.

There are steep gradients in C_n/σ at y = ±1D and it is not clear whether these are produced by the tail rotor or main rotor. The increased C_n/σ at y = 1D and reduced C_n/σ at y = -1D are consistent with increased and reduced tail rotor effectiveness respectively due to the lateral components of the circulation interacting with the tail rotor similar to the upwash interaction with the main rotor. However, the tail rotor is considered too far removed (0.5D) from the vortex centre for there to be sufficient lateral velocity components to produce the measured interaction. It is felt that a more likely explanation is changes in main rotor torque due to the vortices interacting with the blade tips at these locations.

While the response of the helicopter is attributable in several respects to single identifiable dominant phenomena, the wake interference represents a complex flow-field interacting with a dynamic system that is strongly coupled which tends to obscure some of the mechanisms involved. The simplistic arguments used above may not be appropriate. The change in C_Y/σ for instance, is not understood and is probably a cross coupling effect due to the rotor blade dynamics. These arguments are also only based on a linear traverse through the wake. Further insight should be gained in the planar traverses that follow.

The results of a traverse in the y-z plane through the wake from the upwind helicopter are given in Figure 7. The y-z plane was located at x/D = -1.5 and the test conditions were C_T'/σ = 0.035 and μ = 0.10. For the purposes of determining the Δ values it was assumed that the trim values for the force and moment coefficients corresponded to the average of the coefficients along the port edge of the y-z plane, i.e. for y = -1.3D.

There are clear, measurable wake interaction effects that are produced that generally confirm what was measured in the linear traverses of Figure 6 although the advance ratio is different. As before, two distinct regions of increased $\Delta C_T'/\sigma$ exist at the edges of the paths of the trailing vortex pair and between these two maxima lies a significant reduction in $\Delta C_T'/\sigma$ due to the main rotor downwash. There are corresponding increases and decreases in $\Delta C_D/\sigma$ as the main rotor thrust changes produce increases and decreases in propulsive thrust.

Again, there are four distinct maxima in $\Delta C_m/\sigma$, but the two central peaks are dominant. The interference on the starboard side appears slightly greater than found on the port side and there appears to be an asymmetry in the distribution of the peak interference effects about the wake axis. The coupling that was seemed to exist between C_m/σ and C_D/σ in Figure 6 was not supported in Figure 7 which indicates that $\Delta C_D/\sigma$ is produced by the changes in the main rotor thrust.

The wake interference effect produced on $\Delta C_n/\sigma$ is also evident on $\Delta C_Y/\sigma$ at the same locations which are y = ± 0.5D and z = -0.4D. There is also a low magnitude correlation response evident in $\Delta C_l/\sigma$. This coupled response suggests that it is from the tail rotor which is further supported by these locations being somewhat lower down and closer spaced than was the case for the peaks in $\Delta C_T'/\sigma$. All of this is consistent with the trailing vortices passing over the main rotor and "striking" the tail rotor and/or vertical stabilizer. The spikes that may have been expected in $\Delta C_n/\sigma$ at ±1D based on Figure 6 did not materialise.

There are two additional high interference regions evident in $\Delta C_Y/\sigma$ *above* the upwind helicopter that are not understood. This was not an anomaly and was consistently noticed in the test data not presented here. Also, the mechanism producing the three interference zones at z = 0D in $\Delta C_l/\sigma$ is not understood.

Several of the interference zones in Figure 7 appear to "sloping downward" to the starboard side. This is consistent with the roll attitude (to starboard) of the helicopters.

These results were typical of what was measured under different conditions and downwind locations. For example, the changes measured from trim for C_T'/σ with increasing distance downwind from the upwind helicopter are shown in Figure 8. The results show strong consistency and serve to confirm the results in Figure 7. The downwash action is evident as the wake interference zones are convected downwards with increasing downwind distance from the upwind helicopter.

Results for the tests to measure the power required for trimmed flight are shown in Figures 9 to 11. Figure 9 shows the variations produced in C_T' in the presence of the wake interference when the controls and attitude were fixed. Figure 10 shows the measured C_T' in the same region and for the same conditions when the active trim control was engaged. The control algorithm was successful in maintaining a relatively constant C_T'. The changes in the supply current to the motor in this process were recorded and the resulting power coefficient (C_P/σ) is plotted in Figure 11. There is a clear reduction in C_P/σ corresponding to the prominent region of increased C_T' visible in Figure 7 at y/D ≈ -1. There is a contour in Figure 7 where C_T' is unchanged from the free air case. The corresponding C_P/σ for this location was approximately 0.0043. This was used as the boundary for indicating the regions of power reduction and any values less than this threshold are plotted as dashed lines in Figure 11. The minimum C_P/σ is of the order of 0.0038 which represents a savings of approximately 12% over the free air power level. This peak exists over a zone of relatively small size. The tolerance of some flight control system to utilise this benefit would likely be hard pressed to maintain the position and therefore the likely gains will be somewhat less than this value.

Conclusions

The influence of a helicopter wake on the forces and moments on a helicopter operating downwind were successfully quantified experimentally. These results showed that regions of beneficial aerodynamic interference existed, that they were significant in magnitude and that they were consistent. All forces and moments were shown to be affected although the mechanisms producing the measured effects are not all clear.

A power saving of ~12% was measured by tethered trimmed flight of a helicopter model in the upwash outboard from the wake vortex of an upwind helicopter model.

These results indicate that there is significant benefit to be obtained by flying helicopters in correct formations when flying in groups to save fuel over long trips. This is possible because the regions of beneficial influence are in areas which will allow for safe flight operations, especially in VFR conditions and also because the lateral and vertical extent of positive benefit is large enough that correct formation could be maintained by pilots without excessive pilot workload.

Further study is therefore recommended to quantify these benefits more accurately with more representative models and test conditions.

References

[1] Ghee, T A, Berry, J D, Zori, L A J, Elliot, J W, "Wake Geometry Measurements and Analytical Calculations on a Small-Scale Rotor Model", NASA TP3584, ATCOM TR-96-A-007, August 1996

[2] Denton, T.J., Martins, J.C.F., Ratner, G.R., and Skinner, P.J., "Experimental Characterisation and Comparison of a Model Helicopter Rotor Tip Vortex and Fixed Wing Tip Vortex", 29th European Rotorcraft Forum, Germany

[3] Vicroy, D D, Brandon, J, Greene, G, Rivers, R, Shah, G, Stewart, E, Stuever, R, "Characterizing the Hazard of a Wake Vortex Encounter", AIAA paper

[4] Hansen, J.L., and Cobleigh, B.R., "Induced Moment Effects of Formation Flight Using Two F/A-18 Aircraft", NASA/TM-2002-210732

[5] Johnson, W., Derby, M.R. Yamauchi, G.K., Wadcock A.J., "Wind Tunnel Measurements and Calculations of Aerodynamic Interactions between Tiltrotor Aircraft", 41st Aerospace Sciences Meeting and Exhibit, Reno, Nevada, January 6-9, 2003

[6] Padfield, G.D., Manimala, B., Turner, G.P., "A Severity Analysis for Rotorcraft Encounters with Vortex Wakes", Journal of the American Helicopter Society, October 2004, Volume 49 – Number 4, pp 445 – 456.

Figure 1 The two RC helicopter models in the wind tunnel with the upwind helicopter on a fixed strut and the downwind helicopter on the traverse system

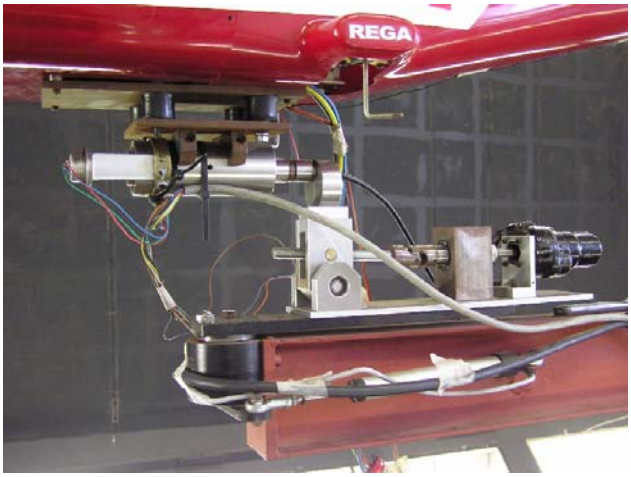

Figure 2 Downwind helicopter support assembly

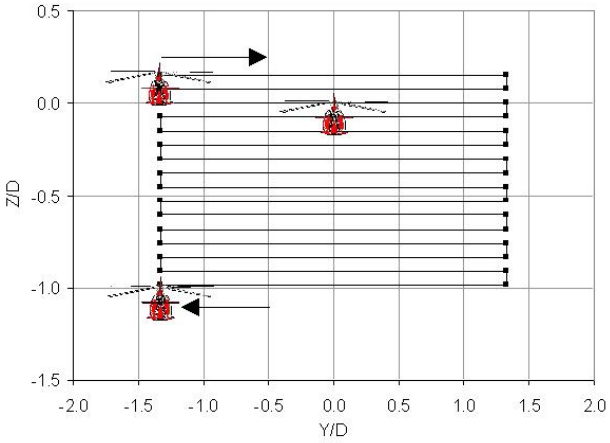

Figure 3 Traverse pattern of the downwind helicopter in the vertical plane; upwind helicopter position indicated at Y/D=0 and Z/D=0

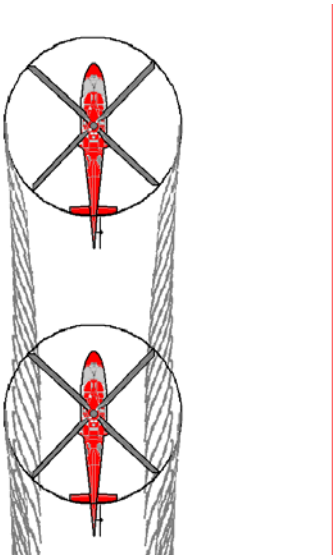

a) y/D = 0

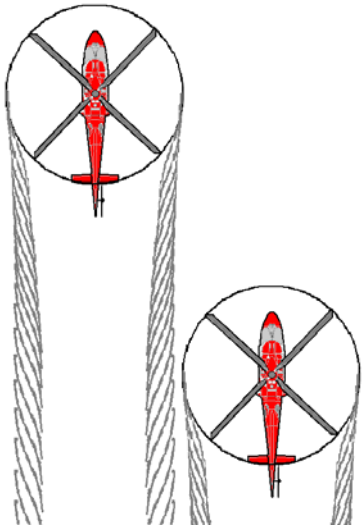

b) y/D = 1

Figure 4 Coordinate convention

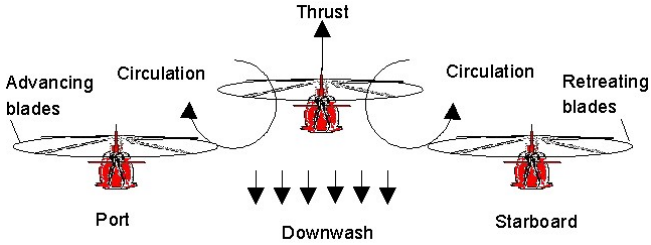

Figure 5 Flow interaction between upwind helicopter and downwind helicopter on port and starboard sides (looking upwind)

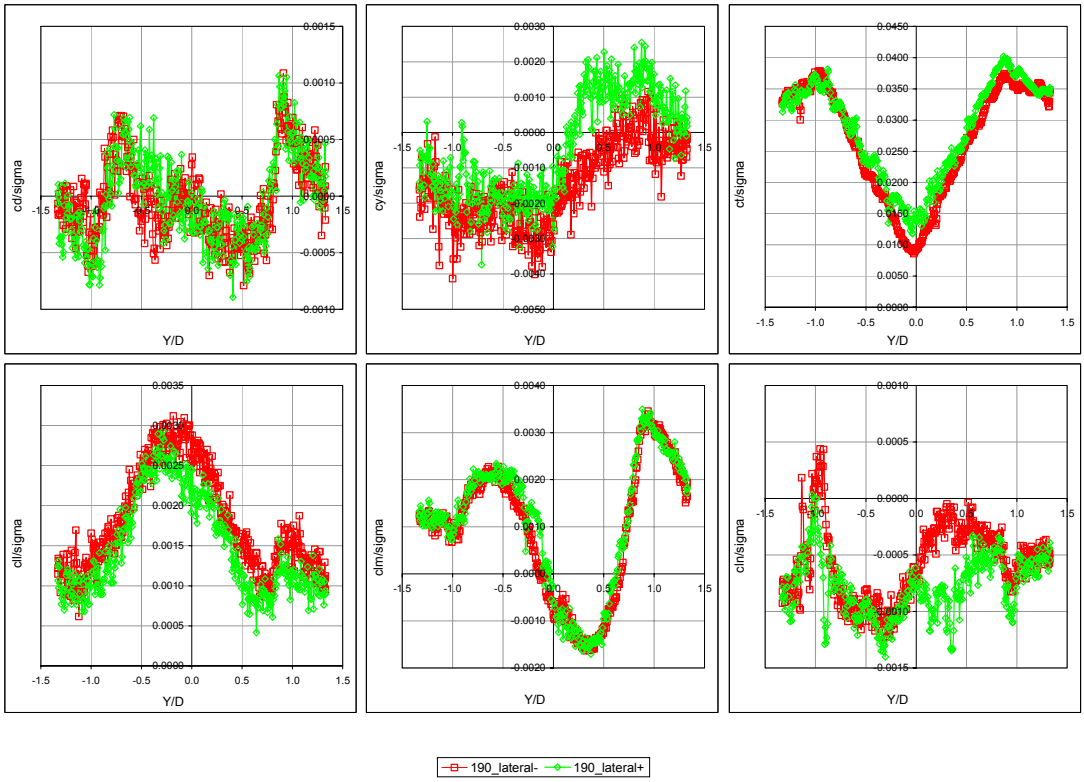

Figure 6 Repeatability of traverses of the downwind helicopter moving continuously in a positive and negative lateral direction at 1.3D downwind and 0.38D below the upwind helicopter; C_T'/σ = 0.035; μ = 0.05

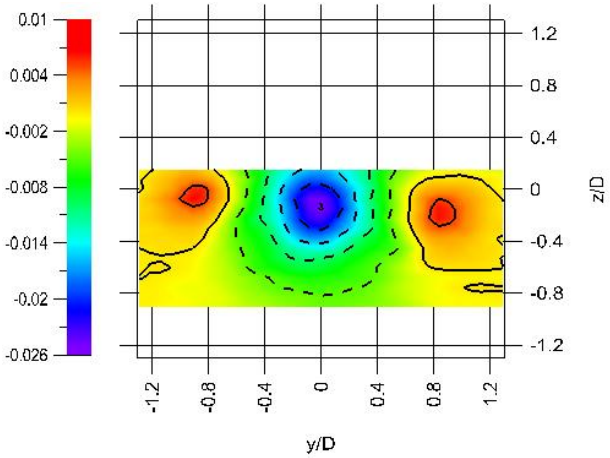

a) $\Delta C_T'/\sigma$; contour increment = 0.005

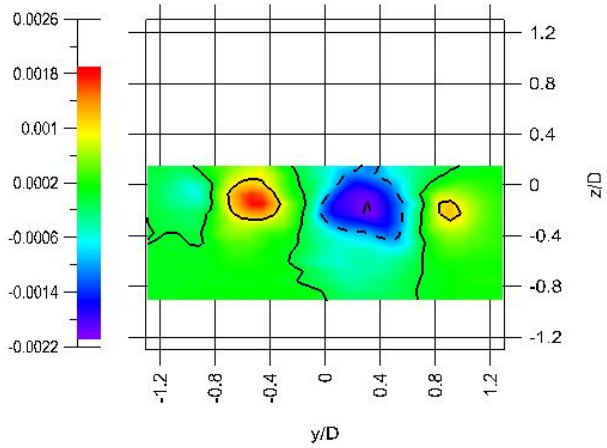

b) $\Delta C_m/\sigma$

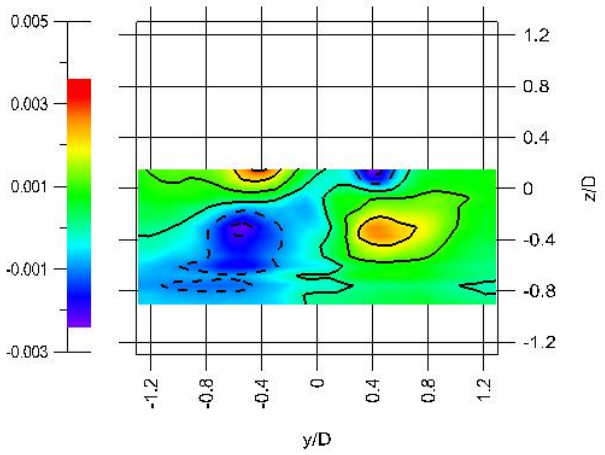

c) $\Delta C_Y/\sigma$

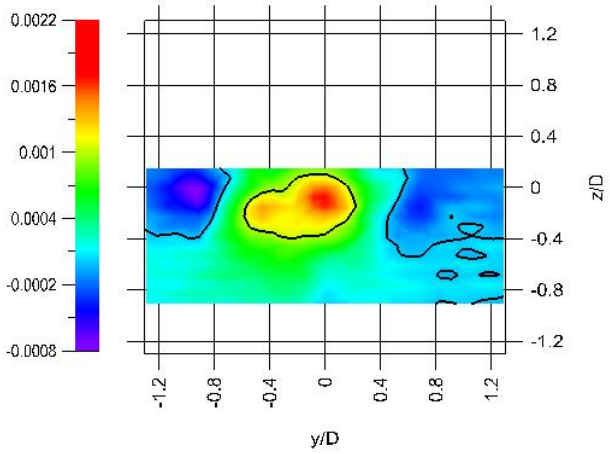

f) $\Delta C_D/\sigma$

Figure 7 Measured force and moment coefficient changes from trim in y-z plane for x/D = -1.5; μ = 0.10; C_T'/σ = 0.035 (contour increment = 0.001, dashed line for negative)

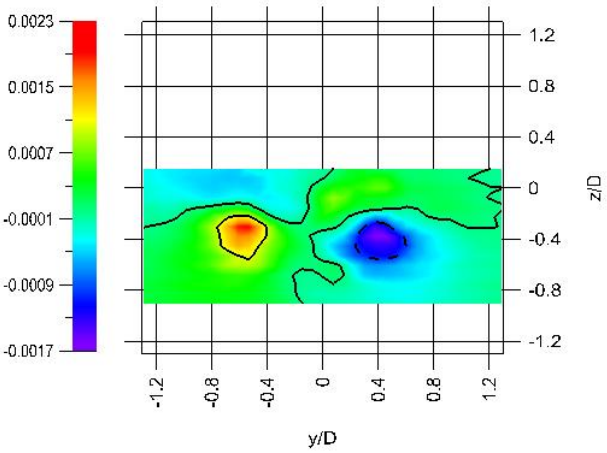

d) $\Delta C_n/\sigma$

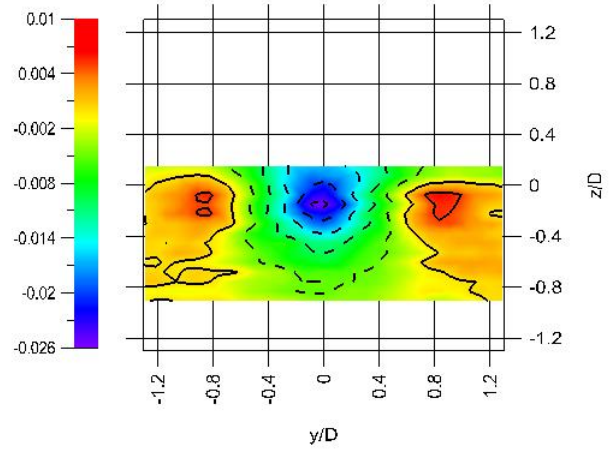

a) x = -2D

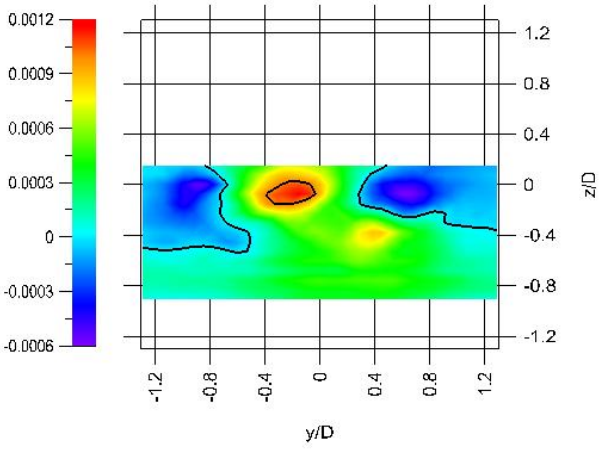

e) $\Delta C_l/\sigma$

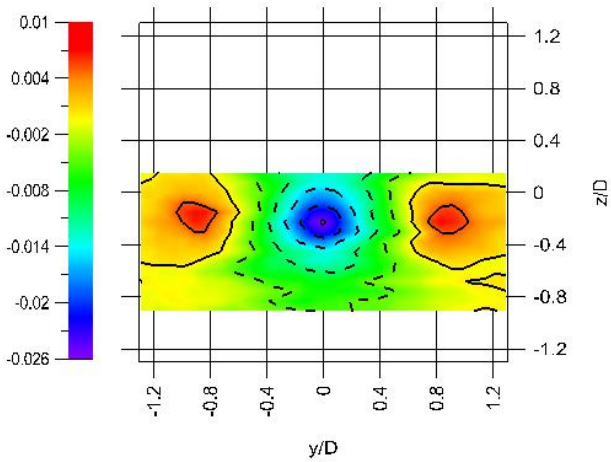

b) x = -3D

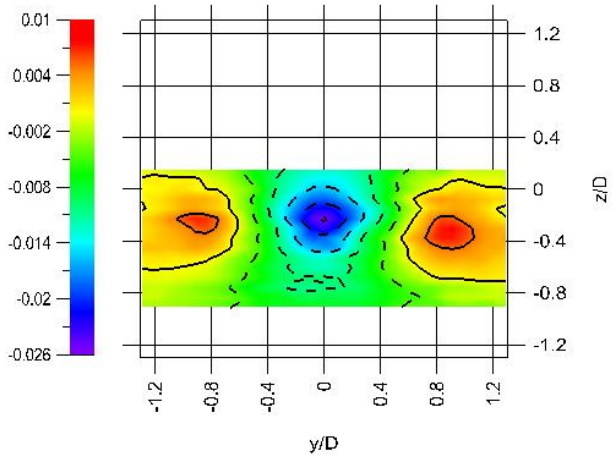

c) x = -4D

Figure 8 Measured $\Delta C_T'/\sigma$ of downwind helicopter in y-z plane as function of distance downwind from upwind helicopter; μ = 0.10; C_T'/σ = 0.035 (contour increment = 0.005, dashed line for negative)

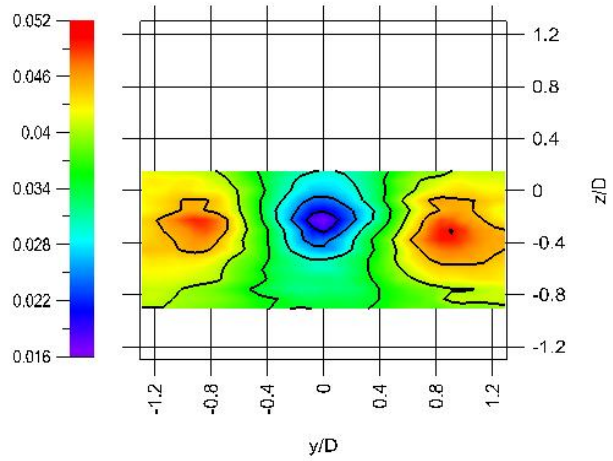

Figure 9 C_T'/σ for traverse with controls locked showing vortex wake interference; x = -4D; μ = 0.10; C_T'/σ free flight = 0.035

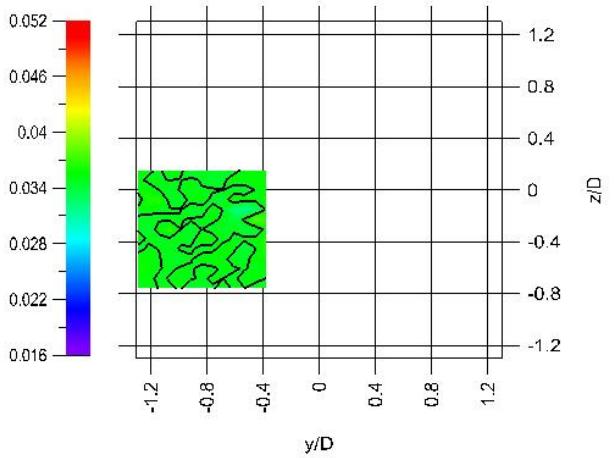

Figure 10 C_T'/σ for traverse with auto trim active; x = -4D; μ = 0.10; C_T'/σ free flight = 0.035

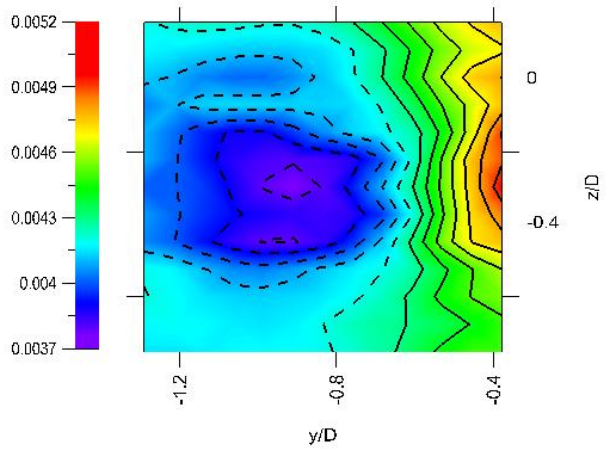

Figure 11 C_P/σ for trimmed flight in vortex wake interference; x = -4D; μ = 0.10; C_T'/σ = 0.035 (contour increment = 0.0001, estimated free flight C_P/σ = 0.0043; dashed line for C_P/σ < 0.0043 where power saving exists)